

Measure of the water pressure during the pressuremeter test in a calibration chamber – Physical and numerical approaches.

P.G. Karagiannopoulos

Jean Lutz SA, Jurançon, France, pkaragiannopoulos@jeanlutzsa.com,

M. Peronne

Jean Lutz SA, Jurançon, France, mperonne@jeanlutzsa.com

P. Reiffsteck

Univ. Gustave Eiffel, IFSTTAR, Marne La Vallée, France, philippe.reiffsteck@ifsttar.fr

ABSTRACT: The knowledge of the pore pressure field evolution around the pressuremeter probe during an expansion test can help to better control the drainage conditions during the test and thus its interpretation, but it can also improve a soil classification method like the one developed for the CPTu. This paper presents the calibration chamber developed by Jean Lutz SA. This device was used to perform pore pressure dissipation tests during the expansion test. The tank has a set of pore pressure and total pressure sensors installed in the ground mass close to the probe. Thus, the variation of the pore pressure could be monitored at different points in real time around the pressuremeter. This paper presents the first experimental data from monotonous and cyclic tests on Hostun sand and compares them with a numerical model (Cesar LCPC) which uses the Mohr coulomb failure criterion elastoplastic model for the soil modelling. Finally, a comparison of the classical triaxial tests with the first multi-cyclic results performed in this calibration chamber is done in order to evaluate the behaviour of the soil under cyclic solicitation and furthermore, the potential risk of soil liquefaction.

Keywords: pore pressure, pressuremeter test, calibration chamber, expansion test analysis.

1. Introduction

The idea of the pore water measurement during the pressuremeter test is based on the Terzaghi's principle. Fig. 1 shows the diminution of the pore pressure and its transformation to effective stress pressure according to the time.

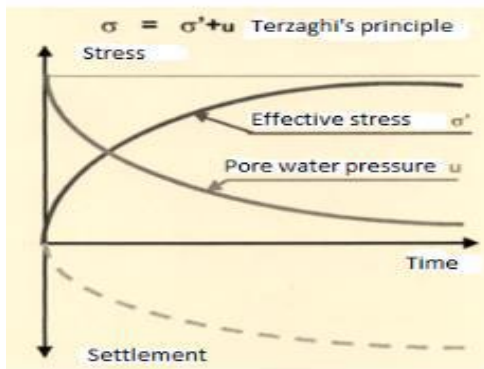


Figure 1. Terzaghi's principle for the stress distribution.

The Menard pressuremeter test with its actual design measures only the total pressure applied to the soil and does not give us any information about the amount of the effective and pore water pressures.

The main purpose of this study is to create a controlled environment (calibration chamber) in which we can measure the variations of the total and pore pressures around the probe. In addition, we can impose the drainage conditions of the experiment and simulate different depths by applying lateral and vertical stresses to the sample like in the classical triaxial test.

2. Description of the calibration chamber

2.1. Design

A watertight tank has been built in the headquarters of Jean Lutz SA which allows to have an experimental approach of the pressuremeter test with the measure of the pore water pressure and total pressure at different distances around the probe. In this way, experimental simulation has been performed in the lab in order to interpret the sand behaviour under monotonous and cyclic stress.

Sensors of the water pore and total pressures are placed inside the sample as shown in Fig. 7. In this way, the variation of the total and water pore pressures during the pressuremeter test and its distribution with the distance to the probe can be observed.

For the application of the lateral and vertical stresses to the sample, two airbags for the vertical stress and one airbag for the lateral stress are used to simulate the in-situ conditions. The Fig. 2 is a picture of those airbags that can be inflated up to 10 bars.



Figure 2. Airbags for the simulation of the lateral and vertical stresses.

The height of the chamber is 72 cm, the diameter is 90 cm so at least 15 times the diameter of the probe. There is an axisymmetry in the chamber around the axis of the probe which is fixed in the centre of the tank with brass nipples as presented in Fig. 3.



Figure 3. Sieves for the sand pluviation (No. 6 et No. 8) and fixed probe in the centre of the chamber.



Figure 4. Calibration chamber and lab equipment.

2.2. Characteristics of the Hostun sand

The Hostun sand is a reference sand for many research in physical modelling (calibration chamber and centrifuge testing) as Toyoura, Ottawa and Ticino sands. The particle size distribution used in this research is referred as the Hostun RF sand in the research papers and classified by the producer as Hostun sand 31. The number 31 is the biggest sieve modulus from which all the grain sizes can pass. Fig. 5 shows the particle size distribution curve of this sand.

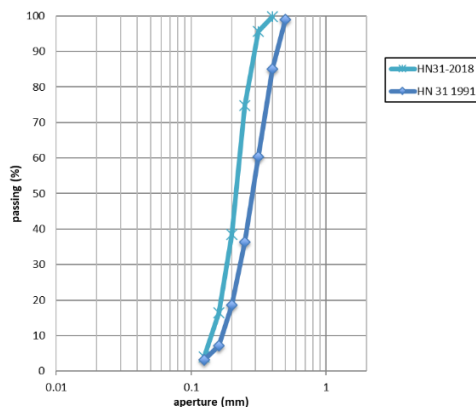


Figure 5. Granulometric curve of the Hostun sand 3.1

The chemical consistence of the Hostun Sand 31 is primarily silice (99.17%) with traces of aluminium, titanium and iron oxide, lime, magnesium, potash and sodium.

The mean grain D_{50} is around 0.35mm which classifies the Hostun sand as a medium sand in the geotechnical classification.

The void ratio ranges between $e_{min}=0.624-0.648$ and $e_{max}=0.961-1.041$ (according to Flavigny et al, [2]). Taking into consideration the grain density of $2.65g/cm^3$, it is deduced $\gamma_{max}\approx 16kN/m^3$ and $\gamma_{min}\approx 13.10kN/m^3$. These values were taken as the maximum and minimum density to calculate the relative density I_D of each experiment.

2.3. Sample reconstitution

The deposition of the soil is done by pluviation using the sieves no. 6 (3.36mm) and no. 8 (2.38mm).

A grain auger screw elevator with an adjustable flow is used for the sand deposition and can be seen in Fig. 4. Thus, the parameters which control the sample density are the grain auger flow in combination with the adjustment of the pluviation height. Verifications of the real density are performed during the pluviation of every specimen and in this way the real density can be found.



Figure 6. Preparation of the experiment and setting up of the sensors.

The sand is dumped by pluviation with the probe fixed in the centre of the tank and the wires of the sensors with cable glands under its base and lid as shown in Fig. 6.

The sensors placed in the tank are either of total or pore water pressure. In total, 5 total pressure sensors and 4 pore water pressure sensors are installed in different locations inside the calibration chamber (their position is explained in Fig. 7). More precisely the sensors are installed close to each airbag in order to measure the real pressure transmitted to the sample. Furthermore, one pore water pressure sensor is placed next to the probe to simulate the sensor placed in the prototype for the in-situ measurements. A companion paper in this conference [10] aims to explain the tests made with this installation.

The pore and total pressure sensors are placed inside the sample symmetrically around the fixed probe in order to minimize their size's impact to the homogeneity of the sand sample.

For every experiment a first calibration of the sand density is carried out with a small container in order to define the deposition intensity and the falling height. Other factors like shutter porosity, shutter-hole pattern, vertical stress on shutter falling distance, distance between diffuser sieves, diffuser sieve opening, and the number of diffuser sieves can have an impact on the density of the sample. However, according to the bibliography and the studies already performed about the pluviation of samples in the laboratory, the main factors which determine the sand density are the

deposition intensity and in a lower level the pluviation height or distance between the sieves and the sample [3, 8].

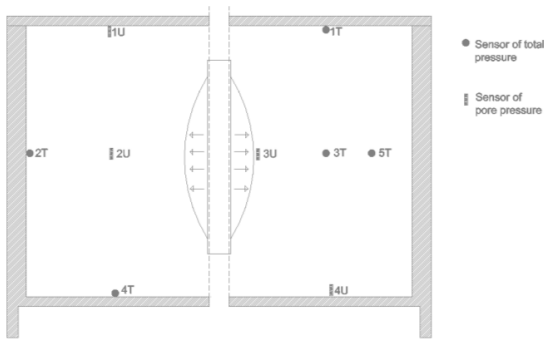


Figure 7. Position of the sensors inside the specimen.

For this reason, only these two factors (flow of the sand and falling height) varied to get a wide range of densities. For the control of the flow, a power inverter was installed which allows to vary the rotation speed of the grain auger and thus, the flow of the sand deposition. There are 11 levels of speed on the whole range as described in table 1.

In order to achieve a looser sand $I_D < 0.4$, we used the method of moist tamping. This wet deposit creates a kind of honeycomb structure resulting from a capillary cohesion and consequently, this structure can create looser samples with a density close to $I_D = 0$. For this type of sand deposition, the impact of the pluviation height is negligible and the method of sand pouring was used. A compaction of the deposited sand is required in order to achieve the relatively most dense sand with a relative density close to $I_D = 0.4$.

Table 1: Results of the deposition methods.

Method	Rotation speed or compaction (dimensionless)	Pluviation height (cm)	Density γ/I_D (KN/m^3)
Dry pluviation	7/11	60	14.5/0.46
Dry pluviation	7/11	30	14.3/0.41
Dry pluviation	1/11	60	15.9/0.97
Dry pluviation	1/11	30	15.6/0.87
Pouring	No	-	12.5/-0.2
Pouring	Yes partially	-	13.1/0
Pouring	Yes	-	14/0.31

We have to notice that for technical reasons we cannot have a speed superior to 7/11 because the grain auger is shaking too much. In addition to this, the level of the sample's compaction, when the sand is poured, cannot be measured with an objective factor but only with the obtained result (sample density).

Generally, in our study we examine the different behaviour between the highly dense ($I_D \approx 1$) and very loose sand ($I_D \approx 0$). In this way, we can easily distinguish the role of the density on the rheological behaviour of the sand.

Furthermore, the tank is filled with carbonic dioxide gas before the water filling. In this way, we can assure a high level of water saturation, filling the voids between the sand grains with water under pressure ($> 200\text{kPa}$) and dissolving the gas trapped in the pores. However, because of this dissolved gas in the sample water, its compressibility modulus

K_w has to be considered in the numerical and analytical simulation much lower than the typical value of the pure water ($K_w = 2.2\text{ GPa}$) as we will see in the next paragraph dealing with numerical simulation.

2.4. Homogeneity of the stresses in the chamber

In order to check and validate the good performance of our calibration chamber, preliminary tests were performed by setting pressure in the sample and recording in the same time, the total and pore pressure stress developed in different points of the chamber. The result curves are displayed on Fig. 8.

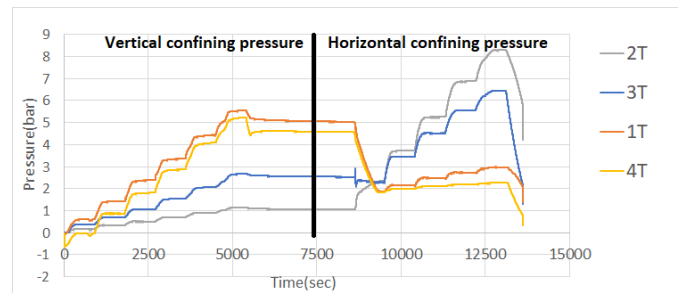


Figure 8. Total pressures in the calibration chamber during dry conditions validation test with steps of 1bar (vertical stresses applied prior to lateral stresses).

The first test was realized in dry sand and the second in completely saturated sand where all the applied pressure from the airbags is transformed to pore pressure. One can compare here the pressures displayed in Fig. 8 and 9.

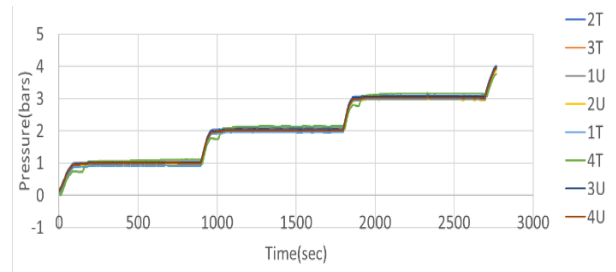


Figure 9. Developed pressures in the saturated sample.

Fig. 9 shows that a complete homogeneous stress field in the saturated sample is obtained. In the dry sample, some small differences in the values of the total stresses are noticed due to the nature of the sand which is not even with the method of reconstitution an isotropic material as the water. In this way, because of the generated local discontinuities around the voluminous stress sensors and the orthotropic character of the sand, we observe these small differences in the stress values.

3. Type of performed tests in the chamber

In this study, at first the repartition of the water pressure is observed, that enables in a second stage to analyze its role. For this reason, we are performing all the 3 types of the equivalent triaxial tests (Consolidated Drained - CD, Consolidated Undrained - CU, Unconsolidated Undrained - UU) examining how the pore pressure is varying and its influence on the pressuremeter parameters. However, taking into account that the soil sample is constituted of

Hostun sand (permeable soil), the type of the experiment which is the most interesting is the consolidated undrained test (CU). In this way, we can generate a pore overpressure during the undrained experiment and examine the influence of the consolidation stress to the different pressuremeter parameters (E_M , p_{IM}). The consolidated drained test is equivalent to a test in a dry sand and the non consolidated undrained test is similar to a CU test with zero consolidation stress (total pressure equivalent to water pressure).

3.1. Dry Monotonous Tests

These tests were performed in order to serve as a reference in the study of the influence of the water on the pressuremeter values (E_M and p_{IM}). In addition, they can be analysed as validation tests for the influence of the border conditions to the experiment's quality.

At first, standard Menard tests were performed in a very high and very low density sand. The pressuremeter results are summarized in the table 2.

Table 2: Pressuremeter values of Menard monotonous test in the calibration chamber.

Density (KN/m ³)	consolidation pressure (σ_h' -bar)	E_M (bar)	P_{IM} (bar)	P1(bar)	P2(bar)
16,03	1	53	7	0,5	5,5
15,7	2	93	12,8	0,5	10,5
16,02	3	179	22,8	0,8	17
12,8	1	22	3,5	0,54	2,5
13	2	36,9	5,75	0,7	3,8
13,2	3	52,2	9	2	6

We can observe that in the Menard pressuremeter test performed in dry sands, the limit pressure is very dependent to the consolidation pressure. Two densities of the sand were examined, the highest and the lowest ones in order to have an obvious contrast in the sand's behaviour. The E_M pressuremeter modulus and the limit pressure have a non linear increase with the increase of the consolidation pressure. The almost constant value of the P1 for the different state parameters (e and σ_h') is probably due to a ground arch effect which is generated by the pluviation of the Hostun dry sand. Thus, the initial pressure around the probe (P1) is reduced and is not equivalent to the consolidation pressure.

Regarding the next graphics Fig. 10, 11 and 12, we can affirm that the dimensions of the chamber are sufficient for the pressuremeter expansion tests taking into consideration that the total pressure close to the border limits does not vary significantly (hypothesis of infinite distance like the in situ conditions).

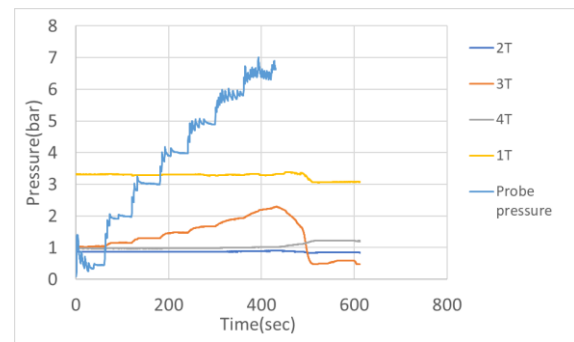


Figure 10. Dry test $\sigma_h'=1$ bar-dense sand.

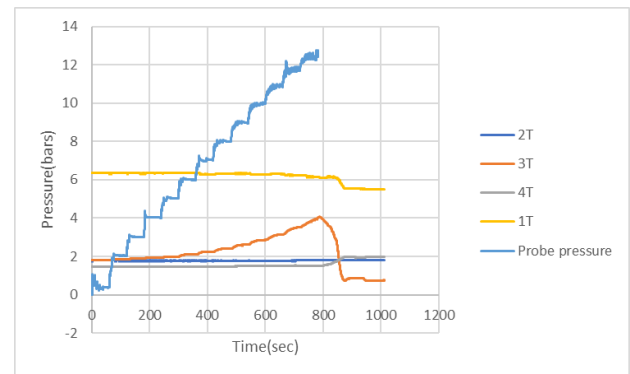


Figure 11. Dry test $\sigma_h'=2$ bar-dense sand.

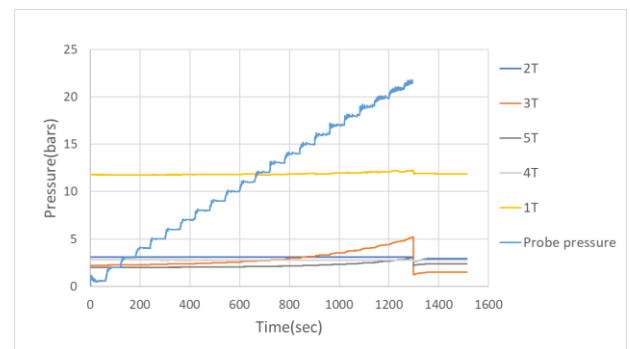


Figure 12. Dry test $\sigma_h'=3$ bar-dense sand.

3.2. CU Monotonous Tests

The same tests with the same state parameter (e, σ_h') were performed in undrained conditions. In this way, we can have the effective stress path during the test and see the potential expansion or contracting phenomena. The purpose of these tests was to examine the influence of the pore water overpressure in the pressuremeter values.

Table 3: Saturated pressuremeter tests.

Case	Density (KN/m ³)	Consolidation pressure (bar)	E_M (bar)	P_{IM} (bar)	P1 (bar)	P2 (bar)
1	15,5	1	53	9,5	2,5	7,8
2	15,85	2	115	18	3,2	14,1
3	15,83	3	140	23	3,8	18
1	12,6	1	17	5,5	2,8	4,66
2	12,8	2	35	8	4,5	6,5
3	12,7	3	78	11,5	5	9

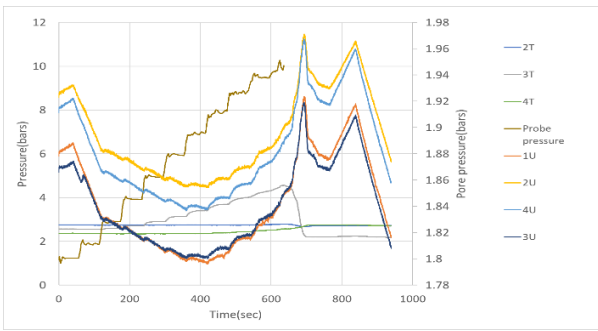


Figure 13. Saturated test $\sigma_h'=1$ bar-dense sand.

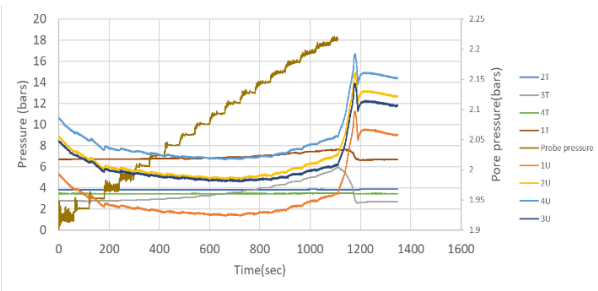


Figure 14. Saturated test $\sigma_h'=2$ bar-dense sand.

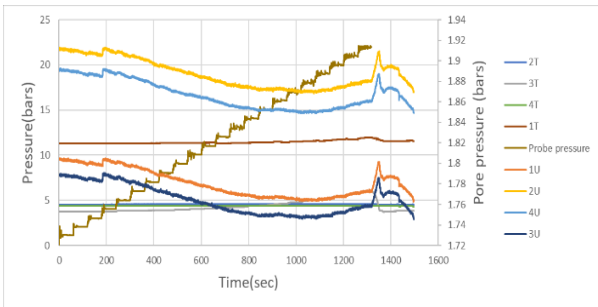


Figure 15. Saturated pressuremeter test $\sigma_h'=3$ bar-dense sand.

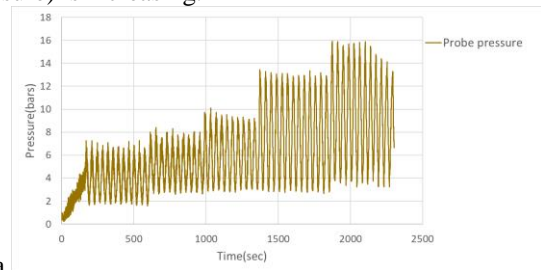
We can distinguish in the table 3 that for the same levels of consolidation, we obtain a higher limit pressure and the pressuremeter modulus E_M stays in similar levels of the dry tests. This increase in the pressure limit can be explained by the presence of the water in the pores which is further less compressible than the existing air in the specimen pores for the dry sands.

After the end of all the saturated experiments, we can observe on Fig. 13, 14 and 15 a pic of the pore overpressure which can be physically interpreted as a phenomenon of an instant cyclical mobility (considerable decrease of the effective pressure) caused by the fast depressurization of the probe in a dilatant sand (impact of a seismic wave). Otherwise, during all the three saturated experiments in the highly dense specimens, we observe a diminution of the pore pressure at the first part of the loading and an increase after the half of the experiment close to the elastic limit (P2). This phenomenon can be interpreted by the alternance of a contractant and dilatant phase of the sand due to the initial high density of the sample (almost the highest one). The decrease of the pore pressure demonstrates the dilatant behaviour of the dense sand and on the contrary, increase is due to its contractant behaviour.

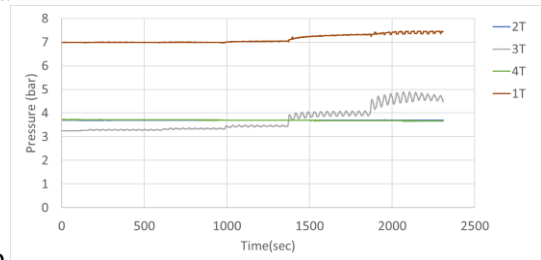
3.3. Cyclic tests-Liquefaction phenomenon

3.3.1. CU tests

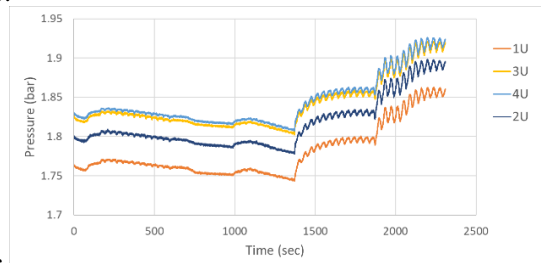
Tests equivalent to the classical triaxial tests CU (consolidated non drained tests) were performed. The consolidation of the dry specimen and the application of the back pressure for the undrained tests were realised before the cyclic loading. In general, we can observe a small hysteresis in the response of the pore pressure to the cyclic loading which can be explained by the rearrangement of the soil grains (contractance of the soil) shortly after the increase in the applied loading as shown in Fig. 16. In this way, the available volume in the soil for the water circulation is decreasing and its pressure (pore pressure) is increasing.



a.



b.



c.

Figure 16. Cyclic test with $\sigma_h'=2$ bar and a back pressure of 1.8bar. Total pressures above (a and b) and pore pressures below (c).

The constant differences of the pore pressures are due to offsets in the zeroing of the sensors.

As observed in the monotonous tests, the total pressure sensors close to the bords of the chamber do not vary significantly during the expansion test in comparison with the sensors placed in the center of the chamber. This result can be considered as a validation of the chamber's dimensions which are sufficient to achieve a relative infinite cavity expansion. The pore pressure varies almost identically in the whole specimen and its value depends especially from the rhythm of the volume accumulation-amplitude of the probe pressure.

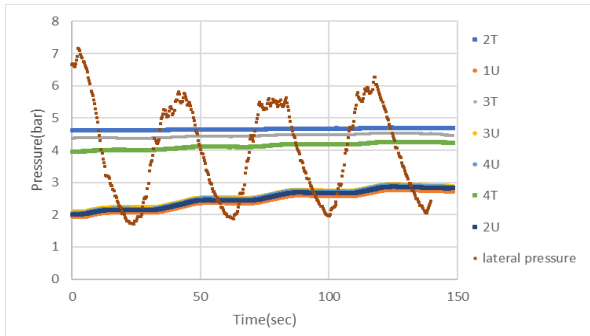


Figure 17. Impact of the cyclic lateral loading to the pore and total pressures inside the chamber $\sigma_h=2$ bar.

We can observe on the Fig. 17 the small increase of the central sensor's value of total pressure in the mid diameter of the chamber in comparison with the applied pressure. This phenomenon is explained by the small influence of the pressuremeter probe in the calibration chamber due to the low probe diameter over chamber diameter ratio. The dimensions of the probe are too small to generate a considerable pore overpressure which can lead to the liquefaction the whole specimen.

Fig. 17 also shows the evolution of the pore pressure for a cyclic variation of the lateral pressure (lateral airbag) which can induce a partial liquefaction of the sand sample.

The pore pressure increases significantly during the lateral cyclic pressure variations (1 bar for 3 cycles) and approaches the total pressure (reduced effective stress). This can be explained by the relative large dimensions of the lateral airbag in comparison with the specimen's volume.

3.3.2. Unconsolidated undrained tests (UU tests)

The pore overpressure during the cycles can be generated with an unconsolidated undrained test in which all the increase of the pressure is taken by the pore water. The unconsolidated sand can be found in the landfills and coastal embankment sites where the deposition of the sand is very recent and the consolidation procedure has not taken place yet. However, it remains a rare case which is too restrictive for the geotechnical design of the civil works. For this reason, most of the time it is preferred to consolidate the soil before the beginning of civil works.

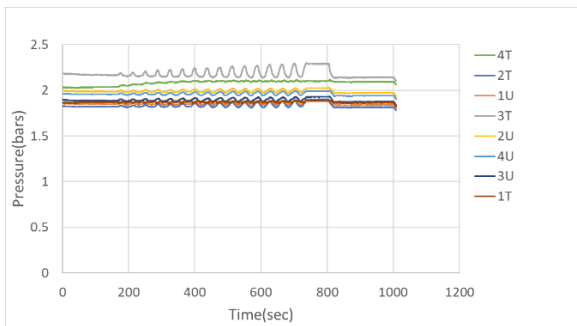


Figure 18. Variations of the total and pore pressure sensors in an UU test (unconsolidated undrained test).

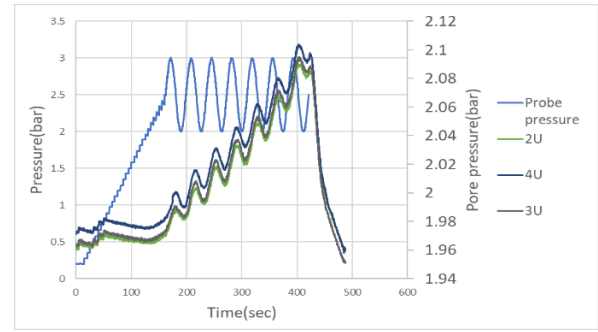


Figure 19. Increase of the pore pressure in an UU specimen (unconsolidated undrained test).

Therefore, it is confirmed from the previous experiments that this type of experiment UU represents a too unfavorable condition and for this reason its results, displayed in Fig. 18 and 19, are not used directly for the calculations of the soil parameters (over-sizing).

3.3.3. Proposed method for the liquefaction risk evaluation

The cyclic loading in undrained conditions can generate a partial liquefaction (cyclic mobility) of the sand. This phenomenon is further studied with cyclic experiments in a loose sand. A series of multicyclic tests is performed in the calibration chamber in order to detect the different parameters which can provoke this complex phenomenon.

In this way, taking into account the existing charts and methods for the evaluation of the liquefaction risk (cyclic triaxial tests, etc.), we further studied the possibility of using the multi-cyclic pressuremeter tests in order to replace the triaxial tests. As we can see in the Fig. 20 and 21, the specimen is loaded cyclically and an envelop curve is drawn for every cyclic test in function of the number of cycles. The number of cycles which corresponds to a cavity deformation equivalent to 50% of the initial volume is defined like the failure criterion of the soil. The volumic deformation and the cyclic stress ratio are calculated by the formulas:

$$\varepsilon_v = \frac{\Delta V}{V_0} = \frac{V - V_1}{V_0}; CSR = \frac{\delta q}{2 * \sigma_c'}$$

V : measured volume of the cavity during the pressuremeter test

V_0 : volume of the initial cavity

V_1 : volume which corresponds to the earth pressure at rest

δq : amplitude of the applied cycle between p_{max} and p_{min}

σ_c' : consolidation stress

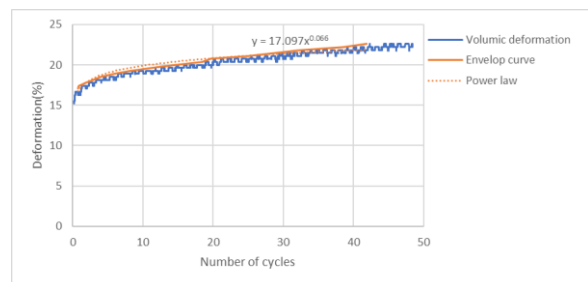


Figure 20. Envelop curve with a ratio CSR=0,1 and a consolidation pressure of 2 bars (completely saturated sample).

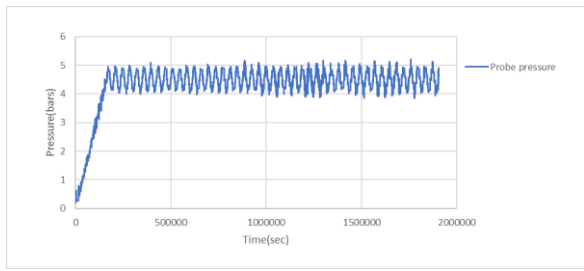


Figure 21. Probe pressure (right) with a ratio CSR=0,1 and a consolidation pressure of 2 bars. (completely saturated sample).

The tests were limited to 50 cycles and if a relative deformation of 50% has not been reached, a power law is fitted to the envelop curve in order to extrapolate the number of cycles for the failure. Cyclic dry and completely saturated tests have been performed in order to distinguish the impact of the water in the evaluation of the risk liquefaction. The figure 21 shows a summary of the carried out tests according to the level of consolidation and saturation.

All the tests shown on the Fig. 22 are carried out in a very loose sand ($I_d=0$) taking into account the results of the triaxial tests which approved that the liquefaction phenomenon can be occurred only in a specimen with a relative density very close to zero. In this way, all these curves correspond to the same initial density but the final density can vary according to the level of consolidation. Some samples taken after the end of these cyclic experiments gave a final relative density $I_d=20-30\%$.

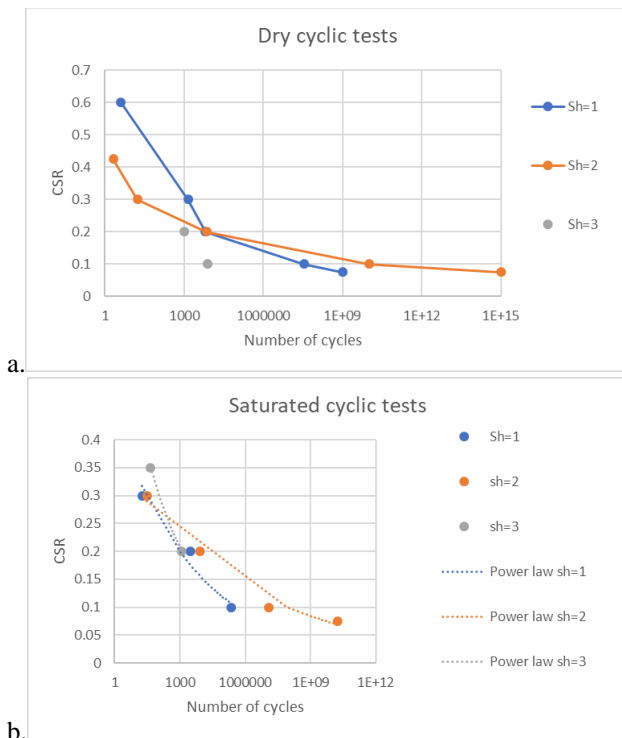


Figure 22. Curves CSR-number of cycles in a loose Hostun sand for different consolidation levels (sh)-dry tests (a) and saturated tests (b).

These tests have to be compared with the triaxial tests performed in the same type of sand and density, in order to define the critical line of the liquefaction. The Fig. 23 shows the results of the triaxial tests taking into consideration all the performed experiments in different densities and granulometries.

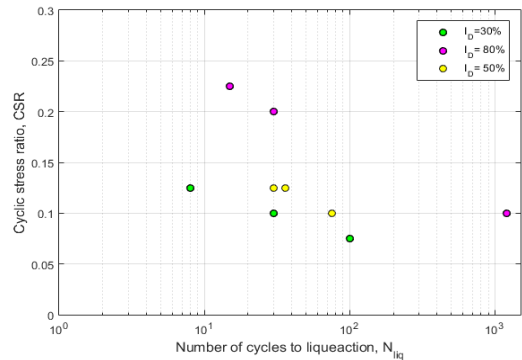


Figure 23. Cyclic triaxial tests for the definition of the critical curve of liquefaction.

3.4. Numerical model

An axisymmetrical model has been created in the finite elements software Cesar – LCPC considering the probe as axis of symmetry. Triangular mesh elements were selected with 3 nodes which means that a linear interpolation is used between the nodes for the displacement calculation.

In order to compare the results in the calibration chamber with the numerical simulation realised with Cesar – LCPC displayed in Fig. 24, we applied the same boundary conditions-level of consolidation and we loaded the specimen by steps applying a final pressure superior to the estimated pressure limit. In this way, we can easily find the level of pressure which leads to a non convergence of the finite element model. To comply with the definition of the limit pressure in the Menard pressuremeter test, we consider as limit pressure, the level of stress in the probe which generates a 12mm deformation of the probe walls (doubling of the cavity for a 60mm probe). As a basis for the comparison, we considered the monotonous tests with the 60mm probe described in the previous chapter.

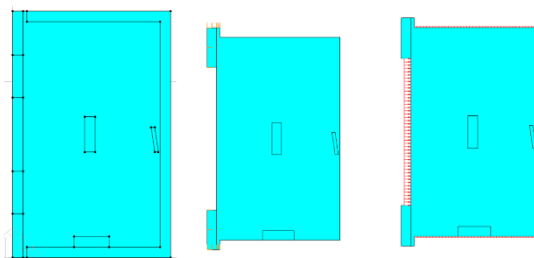


Figure 24. Geometrical model (left), limit conditions (centre) and loading of the specimen (right).

In the first phase, a simple elastoplastic model was used as a rheological model of the soil. More precisely, the Mohr-Coulomb criteria was used considering a cohesion close to zero and a variable friction angle(ϕ) between 37° and 44° according to the soil density. For the dilatancy angle(ψ), a value between 2° and 4° was used for the case of loose sand and 24° to 43° for the dense sand according to the confining stress. Generally, impact of the confining stress is very high and the dilatancy angle is diminished with the increase of this stress.

In this way, taking into consideration these lower and upper limits for the Mohr Coulomb model's parameters without creep, we compare the experimental results with the numerical ones.

For every monotonous dry experiment, described in the previous paragraph, we generated an equivalent model in the finite elements software. The input data, of the deduced pressuremeter values and the comparison with the experimental results in the calibration chamber are resumed in the next tables 4 and 5.

Table 4: Input data of the numerical simulations (c , ϕ , ψ , E_y), deduced limit pressure numerically (Pl) and comparison with the dry tests in the calibration chamber.

l_0	σ_h'	c	ϕ	ψ	E_y	Pl (12mm)	E_y/E_{mcham}	(Pl-Plm)/Plm
100	1	0	41	40	60	7,8	1.25	20%
100	2	0	42	40	180	20	1.45	10%
100	3	0	43	40	220	27,5	1.45	10%
0	1	0	37	2	35	4,3	1.6	20%
0	2	0	37	2	50	7	1.35	20%
0	3	0	37	2	75	11	1.45	20%

Table 5: Input data of the numerical simulations (c , ϕ , ψ , E_y), deduced limit pressure numerically (Pl) and comparison with the saturated tests in the calibration chamber.

l_0	σ_h'	c	ϕ	ψ	E_y	Pl (12mm)	E_y/E_{mcham}	(Pl-Plm)/Plm
100	1	0	40	40	80	8,7	1.51	8%
100	2	0	40	40	150	19,5	1.3	8%
100	3	0	40	40	200	26	1.43	13%
0	1	0	37	2	25	6	1.47	10%
0	2	0	37	2	45	9,5	1.3	18%
0	3	0	37	2	92	14	1.2	21%

The eighth column of the previous tables represents in reality the inverse of the Menard coefficient α and as we can observe it is close to $1/1.45=0.7$ (between 0.6 and 0.8) which is a frequent value for the Hostun sand. Concerning the limit pressure (final column), we can see that the maximum deviation between the numerically and experimentally limit pressure, is inferior to 20%. This uncertainty level is normal and inferior to the security coefficients usually used for the civil engineering works. In this way, we can conclude that with a simple elastoplastic model, we can easily approach the experimental results without performing an exhausting optimization of the input data.

For the undrained case, we chose a model which is independent of the specimen's permeability taking into consideration the experimental results which show an almost simultaneous dissipation of the pore pressure in the whole volume of the specimen. The idea of this modelisation is to decrease the rigidity in compression taking into account the water's compressibility. In this way, we have to introduce in the existing model two new input parameters which are the porosity n and the compression water modulus K_w . The compressibility modulus of the whole specimen is expressed by the formula:

$$K_{tot} = K_{sol} + \frac{K_w}{n} \quad (1)$$

The compressibility modulus of the soil is expressed by the formula:

$$K_{sol} = \frac{E_y}{3*(1-2*\nu)} \quad (2)$$

K_w : compressibility of water, n : efficient porosity of the soil, E_y : Young modulus.

Generally, the second term is largely higher than the first if the value of the pure water is taken into account $K_w=2,2$ GPa. The value of the efficient porosity for the Hostun sand is considered between 0.25 and 0.35. However, considering the value of K_w close to 2,2Gpa the specimen becomes incompressible and its deformations are considerably decreased. Concerning the value of the gas compressibility an approximative value of 2kPa can be considered for the normal ambient conditions. This value is very dependent to the pressure and the temperature of the examined gas. In our case, carbon dioxide gas is injected in the specimen before the application of the water back-pressure. In this way, the dissolution of the gas in the pore water changes very much the water compressibility. For this reason, a value of the water compressibility modulus between 10^5 and 10^6 ($5*10^5$ used value) was retained for our modelisation with a porosity of 0.3.

Concerning the repartition of the total and pore pressures, we can observe qualitatively in figure 24 that it is similar to the physical model. This means that the pressure is highly decreased with the distance from the probe (a ratio of 10 can be deduced between the pressure diminution and the distance of the probe in agreement with the theory). The pore pressure remains constant in the whole specimen after an initial small increase. As we can observe in the Fig. 25, the pore pressure is around 0,25 bar (hydraulic charge of 1m corresponds to 1Pa) in the whole specimen apart from a too narrow zone around the probe which can not be detected with the used sensors in the chamber.

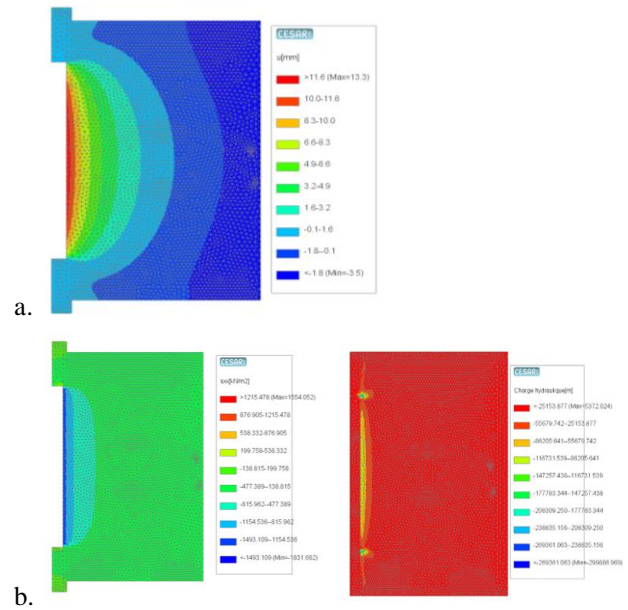


Figure 25. Repartition of the deformation (a), total stresses (b left) and pore pressure (b right).

From the previous results, it is obvious that with a simple axisymetrical model using a basic elastoplastic model (Mohr Coulomb failure criterion) and increasing the rigidity matrix of the soil with the addition of the water compressibility modulus, we can reproduce the experimental results. The comparisons were based on the Menard classical pressuremeter values (pl , E_M') deduced by the monotonous tests. Other rheological models can be

also tested and values in effective pressures can be deduced.

3.5. Conclusions

In this paper, a calibration chamber developed by Jean Lutz SA was presented. The classical Menard probes used in daily practice (60mm and 44mm) were employed for these calibration tests. The Hostun sand was chosen for these first tests taking into consideration that this sand is well documented in the French scientific literature. Monotonous and cyclic tests have been performed in dry or completely saturated specimens. The results of the monotonous tests are compared with an axisymmetrical numerical model in the finite elements software Cesar-LCPC and a non creep elastoplastic Mohr Coulomb failure criterion rheological model was used. The obtained results are very similar and prove the capacity of this simple model to represent the pressuremeter test in the calibration chamber.

Concerning the cyclic tests, a semi-empirical method for the evaluation of the soil's liquefaction risk is proposed by a cyclic loading of the specimen. The results of this method must be compared to the triaxial tests in order to obtain the critical line of soil failure in the CSR-number of cycles diagram for every level of density and consolidation. The measure of the pore pressure during the pressuremeter test is very promising because at a first stage, for the monotonous tests, it can give us an idea of the drainability level of the tested soil and also, provide us with the real effective pressure. The accumulation of the pore pressure during the loading cycles can be used as an index of resistance loss of the soil which can lead potentially to the soil liquefaction. .

The cyclic loading by the probe in the calibration chamber cannot permit us to liquefy the Hostun sand sample because of the small ratio of the probe's diameter to the chamber diameter $D_{chamber}/D_{probe}=15$ to 20 (depending on the used probe 60mm or 44mm). In this way, the induced pressure by the probe to the sample is unable to provoke a significant pore overpressure in the permeable Hostun sand. However, this pressure can be approved sufficient in the case of a clay or silt where an accumulation of the remaining pore pressure is taking place during the cycles in the fined soils (silty clay etc..).

Acknowledgement

The project presented in this article is supported and financed by Jean Lutz SA and ANRT agency. The national project ARSCOP and the Ministry of Ecological and Solidarity Transition have also funded for the Isolate project and the sharing of its results is pretty much appreciated.

References

- [1] Reiffsteck P., Lenti L., Gobbi S., Dang Q.H.- Isolate WP1 M18 Report, 2019
- [2] Flavigny E, Desrues J, Palayer B Note technique : le sable d'Hostun « RF », Revue Francaise de Geotechnique 53:67-70 , 1990, <https://doi.org/10.1051/geotech/1990053067>
- [3] Rad N., Tumay M., Factors Affecting Sand Specimen Preparation by Raining, Geotechnical Testing Journal, Vol. 10, No. 1, 1987,
- [4] Houlsby GT, Hitchman R., Calibration chamber tests of a cone penetrometer in sand, Géotechnique, Vol.38. No.1, pp39-44, 1988, <https://trid.trb.org/view/293793>
- [5] Iskander K., New Pressuremeter Test Analysis Based on Critical State Mechanics, ASCE, Int. J. of Geomechanics pp.625-635 , 2013, <https://ascelibrary.org/doi/10.1061/ASCE GM.1943-5622.0000257>
- [6] Mestat P., Riou Y., Modélisation des sols et des ouvrages avec le modèle Cam-Clay modifié (Modelisation of the soils and the civil works with the modified Cam Clay model), Revue Française de Génie Civil [in French], Taylor Francis, 6 (5), pp.801 – 815, 2002, <https://hal.archives-ouvertes.fr/hal-01007070/document>
- [7] Dano C., Hicher P.-Y., Tailliez S., Varjabédian M., Identification des paramètres de comportement des sols injectés par analyse inverse d'essais pressiométriques (Identification of rheological parameters of the soils with inverse analysis of the pressuremeter tests), Revue Française de Génie Civil , Taylor Francis, 6 (4), pp.631 – 660, 2002, <https://hal.archives-ouvertes.fr/hal-01006938/document>
- [8] Dupla J.C., Application de la sollicitation d'expansion de cavité cylindrique à l'évaluation des caractéristiques de liquéfaction d'un sable.ENPC PHD thesis, 1995, <https://www.theses.fr/1995ENPC9509>
- [9] Benahmed Nadia, Comportment mécanique d'un sable sous cisaillement monotone et cyclique: application au phénomènes de liquéfaction et mobilité cyclique., ENPC PHD thesis, 2001, <http://www.theses.fr/fr/2001ENPC0108>
- [10] Reiffsteck P ,Karagiannopoulos P.G., Peronne M., Dang Q.H, Reiffsteck P, Benoit J, Cyclic pressuremeter tests with pore pressure measurements, application to CSR evaluation, ISC6 Budapest, 2020